5

Electrochemical Reduction, Oxidation and Molecular Ions of 3,3´-bi(2-R-5,5-dimethy-1-4-oxopyrrolinylidene) 1,1´-dioxides

Leonid A. Shundrin
N. N. Vorozhtsov Institute of Organic Chemistry,
Siberian Branch of the Russian Academy of Sciences,
Russian Federation

1. Introduction

An interest in studying of stabilized radical ions of cyclic nitrones is related, first of all, to the problems of revealing possible routes of formation of stable nitroxide radicals from nitrones, which are widely used as spin traps. Some nitrones can undergo reversible one electron electrochemical oxidation to radical cations (RC), and their highly resolved ESR spectra can be obtained in solution at room temperature [1]. In 1992 L. Eberson proposed "Inverted Spin Trapping" mechanism of nitroxide radicals formation, which includes one electron oxidation of initial nitrone to its radical cation (RC) and subsequent reaction with nucleophile [2].

Potentials of the electrochemical reduction (PER) of *N*-oxides vary in rather wide limits: the PER of heteroaromatic *N*-oxides, *viz*., phenazine, acridine, quinoxaline, and pyrazine derivatives, change from –0.85 V to –1.90 V (in DMF *vs*. saturated calomel electrode (s.c.e)) [3,4,5]. In aprotic media, the first step of reductive electrode processes of mono- or *N*,*N*-dioxides is a one electron process. However, the formation of cyclic *N*-oxide's radical anions (RA) stable at 298 K is observed very rare, and the first wave of their reduction is irreversible [4,5-6,7]. The reversible electrochemical reduction (ECR) of 1,1,3-triphenyl-*N*-oxide was mentioned [8]. However, the ESR spectrum of the corresponding RA was not detected down to –40 °C. In turn, the ECR of *N*-oxides of phenazine, acridine, quinoxaline, and pyrazine are characterized by the formation of corresponding RA, and the coupling constants with the ^{14}N nuclei and protons of the aromatic system were determined [3].

In contrast to some types of non nitrone N-oxides described above, ECR of nitrones is irreversible process, and the first step of reduction can be one [4] or two electron [9] by nature. PER of acyclic α-aryl-*N*-alkyl(aryl)nitrones and cyclic nitrones, *viz*., pyrroline and isoindole derivatives, range from –1.80 V to –2.30 V (in DMF *vs*. s.c.e) [6-9]. Published data on the formation of long-lived RA of mono or dinitrones in solution at room temperature are absent.

3,3′-Bi(2-R-5,5-dimethy-1-4-oxopyrrolinylidene)-1,1′-dioxides (**1—4,** Scheme 1), which represent cyclic dinitrones with conjugated C=C bond, are formed by the smooth oxidation of the corresponding pyrrolinones (Scheme 1). Dinitrones **1-4** (DN) have the π-conjugation

chain including both nitrone groups. The extension of the graph of the π-system of the corresponding derivatives compared to the initial pyrrolinones (Scheme 1 (b)) should enhance the electron withdrawing ability of DN **1—4** and, in all probability, favor the stabilization of their RA in enough extent to measure ESR spectra under ECR. Therefore, we studied the peculiarities of ECR and electrochemical oxidation (ECO) of compounds **1—4** in aprotic solvents by cyclic voltammetry. Solvent effects on ECR in MeCN:H_2O mixtures have been studied also.

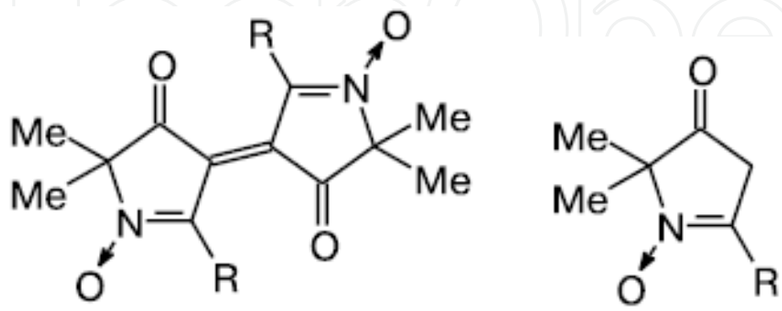

(a) (b)

Scheme 1. Structures of 3,3´-bi(2-R-5,5-dimethy-l-4-oxopyrrolinylidene) 1,1´-dioxides ((R = CF_3 (**1**), Me (**2**), Ph (**3**), Bu^t (**4**)) (*a*) and corresponding initial 2-R-5,5-dimethy-4-oxopyrrolinone-1-oxides (*b*).

2. Experimental

Cyclic voltammograms (CV) of dinitrones **1—4** were measured on CVA-1BM electrochemical system (Bulgaria) equipped with a LAB-MASTER polyfunctional interface (Institute of Nuclear Physics, Novosibirsk, Russia), which enables one complete digital control of the system. Measurements were carried out in a mode of triangular pulse potential sweep in the range of sweep rates 0.1 $V \cdot s^{-1} < v < 50\ V \cdot s^{-1}$. A standard electrochemical cell with a working volume of 5 mL was connected to the system *via* the three electrode scheme and equipped with a salt bridge filling with a supporting electrolyte solution in DMF or MeCN to connect the working volume and reference electrode. The working electrode was a stationary spherical Pt electrode with a surface area of 8 mm^2, a Pt spiral was the auxiliary electrode, and a saturated aqueous calomel electrode (SCE) served as the reference electrode. The supporting electrolyte was Et_4NClO_4 (0.1 mol/dm^3) for aprotic solvents and $LiClO_4$ (0.1 mol/dm^3) for MeCN-H_2O mixtures. Oxygen was removed by passing argon through the working solution. The concentration of depolarizers was $1 \cdot 10^{-3}$ mol/dm^3.

ESR spectra of paramagnetic intermediates of the ECR and ECO processes were measured on a Bruker ESP-300 radio spectrometer equipped with a double resonator. Compounds **1—4** were oxidized and reduced in combination with ESR spectrometric measurements under anaerobic conditions at potentials of the corresponding first reduction or oxidation peaks at T = 298 K in a three electrode electrochemical cell for EPR measurements equipped with a Pt electrode. The space of the working electrode of the cell was placed into the front shoulder of the ESR spectrometer resonator. Numerical simulation of ESR spectra were performed according to the Winsim 2002 program with the SIMPLEX optimization algorithm.

To establish possible structures and of compounds **1—4**, as well as those of their molecular ions (radical anions (RA), radical cations (RC), dianions (DA) and dications (DC)) quantum chemical calculations of the corresponding species were carried out by semiempirical PM3 method (WinMOPAC 7.0 program set) using unrestricted (UHF) and restricted (RHF) Hartree-Fock approximations. Spin density distributions in RA and RC were calculated with DFT/PBE method ("Nature" program set [15]) for gas phase. For RA and RC of DN **2** in gaseous phase and in solution spin density distribution was calculated with (U)B3LYP method using 6-31+G* basis set. PCM model was used to describe the solvent (MeCN of H_2O). All calculations have been done with complete geometry optimization and symmetry restraints for the Me groups in position 5 of the pyrrolinone cycles and for substituents in position 2 according to their local dynamic symmetry (C_{3v}) for the CF_3, Me, and Bu^t groups and C_{2v} for Ph. No restraints were imposed on rotation of all substituents about the pyrrolinone cycles.

3. Results and discussion

3.1 Electrochemical reduction and oxidation of 3,3´-bi(2-R-5,5-dimethy-1-4-oxopyrrolinylidene) 1,1´-dioxides in aprotic solvents

Cyclic voltammograms of DN **1—4** in the region of negative potentials contain two reversible one electron reduction peaks (EE –process) corresponding to the formation of RA and DA (Fig.1, example for DN **1**). The replacement of the DMF [10] solvent by MeCN [11] does not qualitatively change the reduction processes. In MeCN, the potentials of reduction peaks are by approximately 0.1 V shifted to the region of more negative values compared to the potentials measured in DMF (Table1).

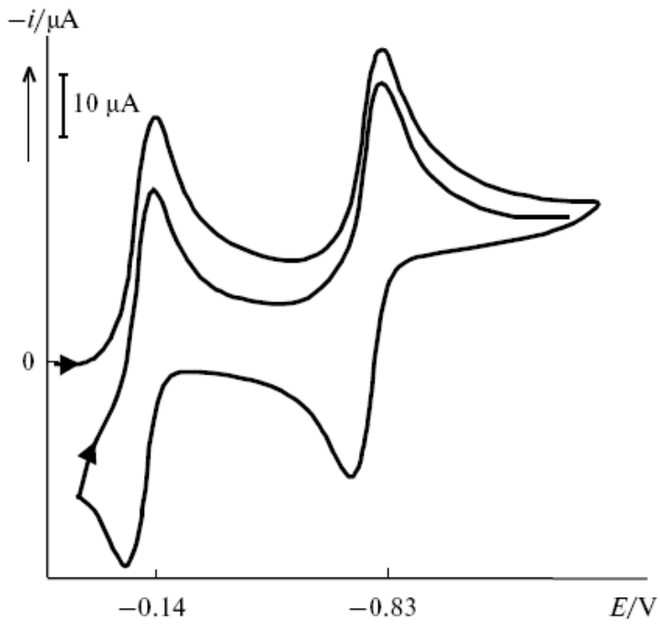

Fig. 1. Cyclic voltammogram of compound **1** (DMF, C=1·10^{-3} mol/dm^3, v = 0.08 V·s^{-1}, supporting electrolyte 0.1 *M* Et_4NClO_4).

The CV of DN **1—4** in the region of positive potentials are shown in Fig. 2. For the potential sweep rate $v < 5$ Vs^{-1}, the CV curve of **1** exhibits the single irreversible oxidation peak. It is most likely that the irreversibility is caused by a fast chemical reaction involving RC. In

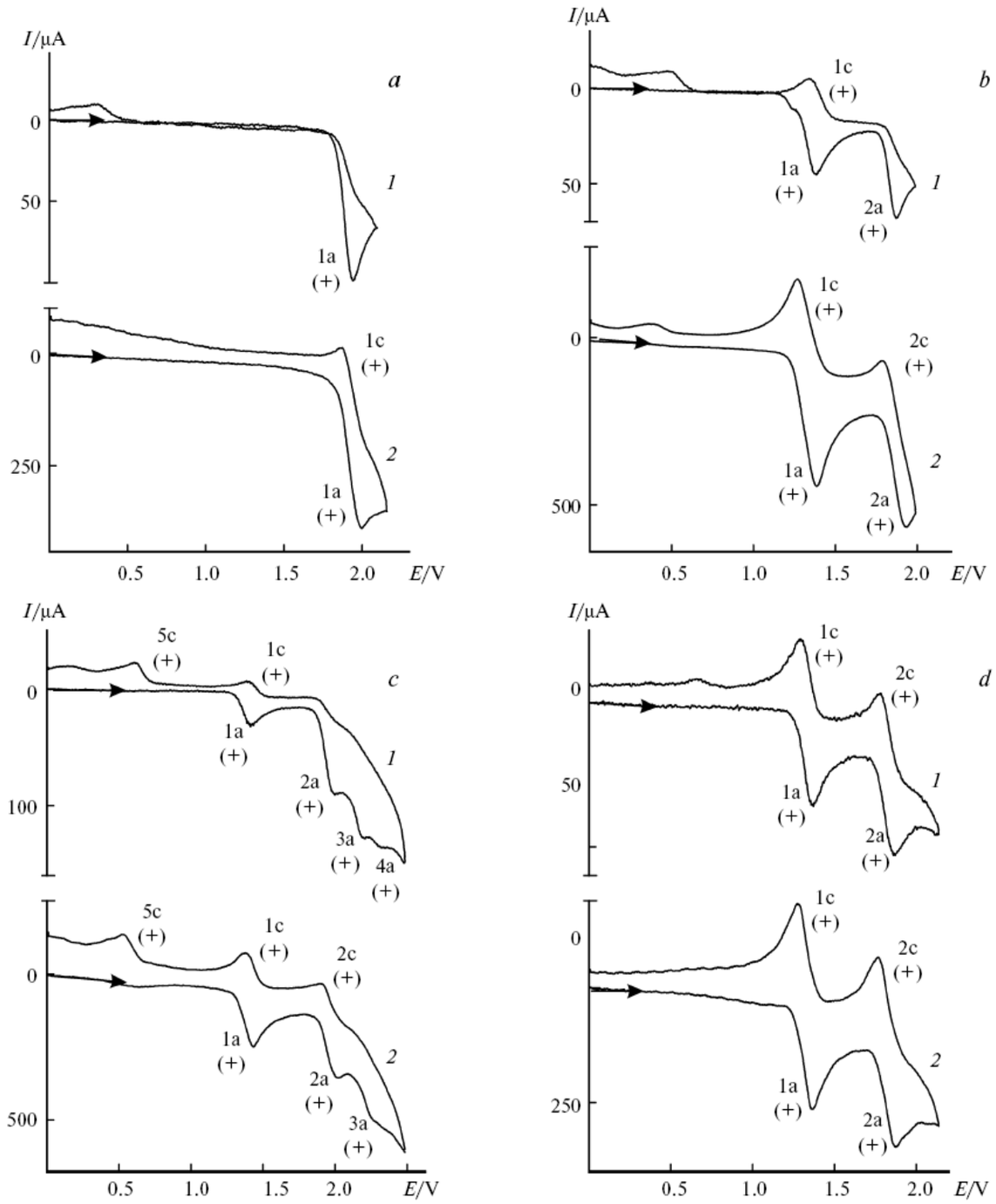

Fig. 2. Cyclic voltammograms of dinitrons **1—4** (*a—d*, respectively) in the region of positive sweep potentials and v = 0.1 (*1*), 5.0 V s^{-1} (2); $C_0 = 1 \cdot 10^{-3}$ mol/dm^3, MeCN, supporting electrolyte 0.1 M Et_4NClO_4.

		Oxidation[a]				Reduction			
№	R	$E_{(+)}^{1a}$	$E_{(+)}^{1c}$	$E_{(+)}^{2a}$	$E_{(+)}^{2c}$	$E_{(-)}^{1c}$	$E_{(-)}^{1a}$	$E_{(-)}^{2c}$	$E_{(-)}^{2a}$
1	CF_3	1.94 (1.98)[b]	- (1.88)	-	-	-0.18 (**-0.13**)[c]	-0.11 (**-0.06**)	-0.81 (**-0.83**)	-0.71 (**-0.76**)
2	CH_3	1.38 (1.39)	1.32 (1.30)	1.88 (1.90)	- (1.80)	-0.58 (**-0.50**)	-0.48 (**-0.43**)	-1.07 (**-1.14**)	-1.00 (**-1.07**)
3	Ph	1.41 (1.41)	1.36 (1.35)	1.98 (2.00)	- (1.89)	-0.55 (**-0.44**)	-0.47 (**-0.37**)	-1.05 (**-1.07**)	-0.95 (**-1.00**)
4	Bu^t	1.36 (1.36)	1.29 (1.26)	1.86 (1.87)	1.78 (1.77)	-0.52 (**-0.47**)	-0.45 (**-0.40**)	-1.00 (**-0.99**)	-0.93 (**-0.92**)

a At the Pt electrode *vs*. SCE in an 0.1 *M* solution of Et_4NClO_4 in MeCN, $C_0 = 1 \cdot 10^{-3}$ mol/dm^3, potential sweep rate 0.1 V s^{-1}.
b Peak potentials at a potential sweep rate of 5 V·s^{-1} are given in parentheses.
c Fist peak potentials in DMF.

Table 1. Peak potentials (V) of electrochemical reduction (MeCN, DMF) and oxidation (MeCN) of compounds **1—4**.

turn, the ECO of dinitrons **2** and **4** is characterized by two peaks, whereas four oxidation peaks are observed for **3**. The observed peaks are characterized here by their potentials in the region of positive ($E_{(+)}^{ij}$) and negative ($E_{(-)}^{ij}$) values, respectively (*i* is the number of peak, and *j* = a or c indicates the anodic or cathodic branch of the CV curve, respectively). The first oxidation peaks of all compounds are diffuse in nature, $I_{(+)}^{1a} \cdot v^{0.5}$ =const, where $I_{(+)}^{1a}$ is the maximum current of the first peak in the anodic branch of the CV.

For compounds **2—4**, the first peaks correspond to the reversible one electron process (ratio of currents of the anodic and cathodic branches $I_{(+)}^{1a}/I_{(+)}^{1c} \approx 1$ and $\Delta E = E_{(+)}^{1a} - E_{(+)}^{1c} = 0.06$ V).

At low sweep rates ($v < 4$ V·s^{-1}), the second oxidation peak of **2** is irreversible, and in the range 5 V·s^{-1} < v < 50 V·s^{-1} the CV of **2** exhibits two reversible one electron peaks (see Fig. 2, *b*). Noticeable instability of DC of **2** formed at the potential of the second oxidation peak is related, most likely, to proton elimination from the methyl group in position 2 (see also Ref. [12]). In fact, when the methyl groups are replaced by the *tert*-butyl groups, the ECO of dinitron **4** in MeCN at $T = 298$ K is an EE process with formation of stable RC and DC in the whole studied range of v (see Fig. 2, *d*). The peak corresponding to the formation of DC **3** is irreversible ($E_{(+)}^{2a}$, $v < 5$ V·s^{-1}, see Fig. 2, *c*), the ratio is $I_{(+)}^{2a}/I_{(+)}^{1a} = 2.57$, and two additional oxidation peaks, whose nature was not studied, are observed in the anodic branch. As in the case of methyl-substituted DN **2**, when v is increased to 5 V·s^{-1}, the $E_{(+)}^{2a}$ peak becomes reversible and one electron in nature ($I_{(+)}^{2a}/I_{(+)}^{1a} = 0.97$), and the $E_{(+)}^{4a}$ peak observed at low potential sweep rates disappears (see Fig, 2, c, curve 2). The irreversible (at all v) peak $E_{(+)}^{5c}$ in the cathodic branch of the CV (Fig.2, *c*) is attributed, most likely, to the ECO of the conversion products of DC **3**, because this peak is not observed for the potential sweep in the range 0 V < E < 1.7 V.

To establish the nature of the oxidation peak of trifluoromethyl substituted DN **1**, we measured the CV in the potential sweep region –1.0 V < E < 2.2 V (Fig. 3, *a*) and in the rate

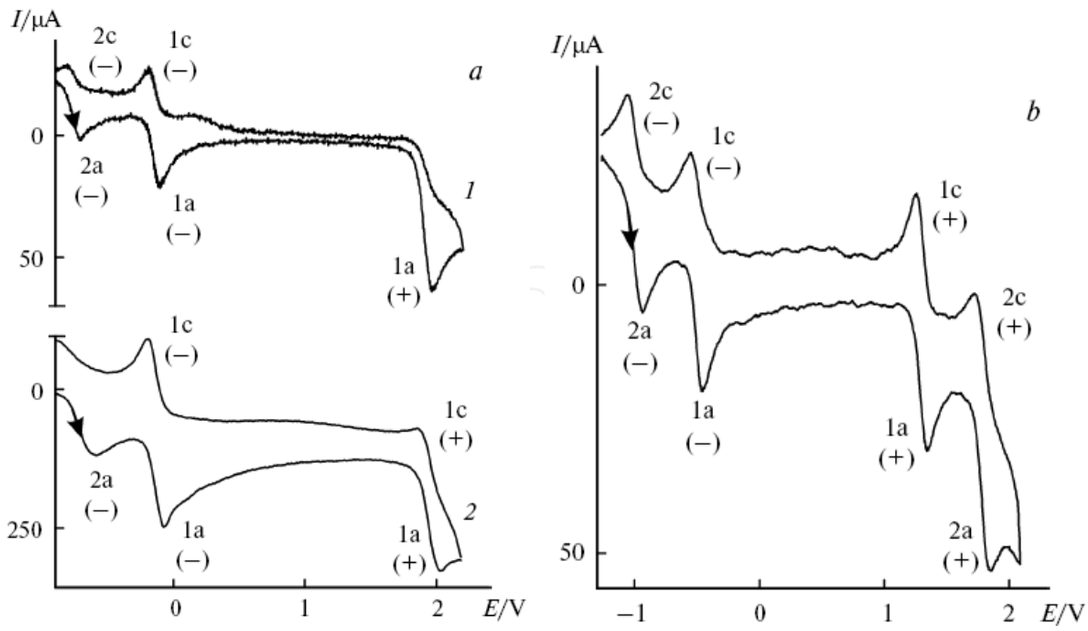

Fig. 3. Cyclic voltammograms of dinitrones **1** (*a*, v = 0.1 (*1*) and 5 V·s^{-1} (*2*)) and **4** (*b*, v = 0.1 V·s^{-1}) in oxidation and reduction areas of potential sweep in MeCN.

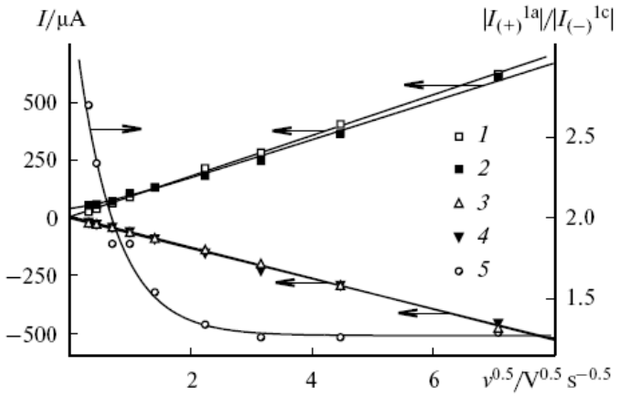

Fig. 4. Currents of the first oxidation ($I_{(+)}^{1a}$) and reduction ($I_{(-)}^{1c}$) peaks of DN **1** (*1*, *3*) and **4** (*2*, *4*) and the ratio $|I_{(+)}^{1a}|/|I_{(-)}^{1c}|$ (*5*) for DN **1** *vs.* $v^{0.5}$.

range 0.1 V·s^{-1} < v < 50 V·s^{-1}. For v = 0.1 V·s^{-1}, the ratio of currents of the observed oxidation peak and reversible one electron reduction peak is $|I_{(+)}^{1a}|/|I_{(-)}^{1c}|$ = 2.7. In the interval of 0.1 V·s^{-1} < v < 10 V·s^{-1}, the ratio decreases exponentially to 1.26 and remains constant up to v = 50 V·s^{-1} (Fig. 4). The plots of currents of the oxidation peak of DN **1** and its first reduction peak corresponding to the formation of RA **1** *vs.* potential sweep rate are shown in Fig. 4 along with similar plots for *tert*-butyl substituted DN **4**, whose all one electron peaks are reversible in both the negative and positive potential regions (see Fig. 3, *b*). The dependences of all currents of the reversible peaks on the potential sweep rate are well described by the classical equation:

$$I_{(\pm)}^{ij} = B + Av^{0.5}, \quad (1)$$

where $A = 0.4463 \cdot S_{el} \cdot (nF)^{3/2}(D/(RT))^{0.5} \cdot C_0$, $n = 1$ is the number of transferred electrons, S_{el} is the surface area of the working electrode, D is the diffusion coefficient of the substance, C_0 is the depolarizer concentration, and B is an empirical constant related to the perturbation of linear free diffusion. The parameters in Eq. (1) A, B, and r^2 (r^2 is the correlation coefficient) have the following values: DN **1**, $I_{(-)}^{1c}$, –67.56 μA·V$^{-0.5}$s$^{0.5}$, 7.73 μA, and 0.998; DN **4**, $I_{(-)}^{1c}$, –65.95 μA V$^{-0.5}$ s$^{0.5}$, –0.33 μA, 0.997, $I_{(+)}^{1a}$, 88.88 μA·V$^{-0.5}$s$^{0.5}$, 4.41 μA, and 0.998.

The dependence of the oxidation peak current of DN **1** on the potential sweep rate is described by the equation:

$$I_{(+)}^{1a} = B + Av^{0.5} + C\exp(-kv^{0.5}), \quad (2)$$

where C and k are empirical constants. The parameters in Eq. (2) for $I_{(+)}^{1a}$ are the following: A = 88.33 μA·V$^{-0.5}$s$^{0.5}$, B = 6.28 μA, C = 35.33 μA, k = 1.48 V$^{-0.5}$s$^{0.5}$, and r^2 = 0.996. The last term in Eq. (2) reflects the contribution of the electrode process associated with the oxidation of the RC **1** conversion products. This process seems to be rather slow in the CV time scale. Hence, for a relatively low increase in v (up to 5 V·s^{-1}), Eq. (2) can rapidly be reduced to Eq. (1), the oxidation peak of **1** becomes reversible and one electron, and the slope (A) of the plot of the peak current *vs.* $v^{0.5}$ is virtually equal to that of $I_{(+)}^{1a}(v^{0.5})$ for **4** (see Fig. 4). In the region of negative potentials, the slopes of the plots of the currents of the first reduction peaks of **1** and **4** ($I_{(-)}^{1c}$) are fairly close (see Fig. 4).

Thus, ECR of DN **1-4** is an EE process in aprotic solvents, whereas ECO is more complicated. The first step of oxidation of DN **1—4** is the one electron transfer to form RC **1—4**. For trifluoromethyl substituted DN **1**, the observed current of the first oxidation peak at low v contains an additional contribution from the electrode process related to the oxidation of the RC **1** conversion products. A similar situation is observed for the second step of oxidation of DN **3**. The second ECO step of DN **2** and **4** is one electron but only DC **4** is noticeably stable.

Note that both ECO and ECR of *tert*-butyl substituted DN **4** are EE processes accompanied by the formation of DA, RA, RC, and DC which are long-lived at T = 298 K (see Fig. 3, *b*). Perhaps, this is the first example of an organic heterocyclic compound for which four long-lived molecular ions were detected within one potential sweep cycle.

3.2 Electrochemical reduction of 3,3´-bi(2-R-5,5-dimethy-1-4-oxopyrrolinylidene) 1,1´-dioxides in MeCN:H_2O mixtures of various composition.

Among dinitrones **1—4**, methyl substituted DN **2** is most water soluble. In a saturated aqueous solution containing the supporting electrolyte $LiClO_4$ (0.1 mol/dm^3) at 25 °C, its concentration (~6·10^{-4} mol/dm^3) is sufficient for the direct CV study of ECR. Due to a lower solubility, the electrochemical reduction potentials of DNs **1, 3, 4** in water were determined by the extrapolation method, starting from the dependences of the reduction potentials on the water content in MeCN—H_2O binary mixtures. The same dependence was studied for comparison for DN **2**.

The transition from the Et_4NClO_4 supporting electrolyte (see Ref. [11]) to $LiClO_4$ shifts the potentials of the first cathodic peaks ($E_{(-)}^{1c}$) measured in MeCN by 0.1 V, on the average, toward less negative potentials. The diffusion nature and reversible one electron character of the first reduction peak are retained upon this transition. The region of reduction potentials

accessible for measurement in MeCN—H_2O binary mixtures is 0.5 V > E > –1.1 V and restricted by the potential of water reduction on Pt under these conditions. When the water content in the binary mixture increases, the potentials of the first reduction peaks of compounds **1—4** shift toward less negative values (Fig. 5, example for DN **2**), reaching in water very low values (Table 2). In all cases, the first peaks are one electron and reversible in the whole range of compositions of MeCN—H_2O mixtures. The plots of the potentials of the first reduction peaks *vs*. MeCN content in the mixture are linear and described by the regressions in the form:

$$E_{(-)}^{1c} = E_{0(-)}^{1c} + A \cdot V_{MeCN}, \quad (3)$$

where V_{MeCN} is the volume fraction of MeCN. The regression parameters A and corresponding correlation coefficients r are given in Table 2. Unlike DN **2—4**, on going from MeCN to H_2O the potential of the first reduction peak of trifluoromethyl derivative **1** lies in the region of positive values *vs*. s.c.e.

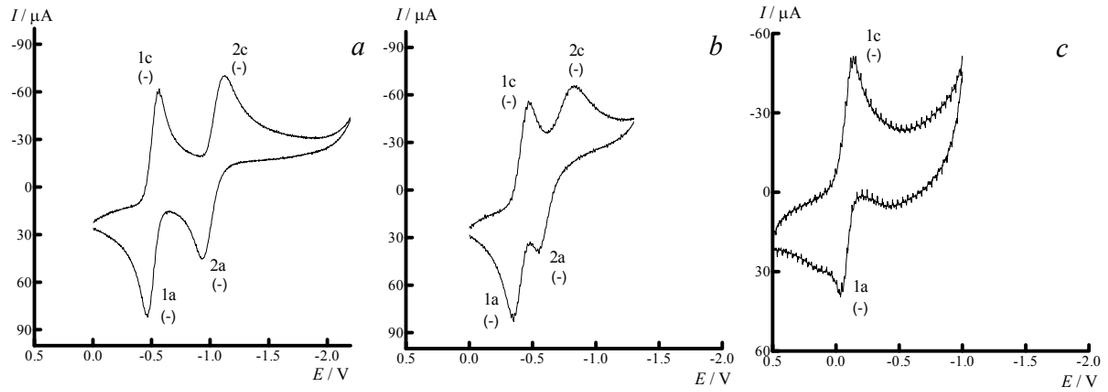

Fig. 5. Cyclic voltammograms of DN **2** in MeCN (*a*), MeCN—H_2O binary mixture (V_{MeCN} = 0.98) (*b*), and H_2O (*c*) (ν = 0.1 V s^{-1}, supporting electrolyte 0.1 *M* solution of $LiClO_4$).

Compound	$E_{0(-)}^{1c}$, V	A, V	r
1	0.19	-0.52	0.989
2	-0.13[b]	-0.35	0.998
3	-0.09	-0.33	0.998
4	-0.08	-0.32	0.998

a Potentials *vs*. SCE at the Pt electrode in a 0.1 *M* solution of $LiClO_4$; ν = 0.1 V· s^{-1}.
b The potential of the first reversible one electron reduction peak measured directly in H_2O at the Pt electrode is –0.14 V *vs*. SCE in a 0.1 *M* solution of $LiClO_4$ at ν = 0.1 V·s^{-1}.

Table 2. Parameters of the linear dependences of the first reduction peaks potentials of DN **1—4** ($E_{(-)}^{1c}$) on MeCN volume fraction in MeCN—H_2O binary mixtures[a] (see Eq. (3)).

The second reversible reduction peak, which is distinctly seen on CV of DN **1—4** in MeCN and related to the formation of the corresponding DA (Fig. 5, *a*) becomes quasi reversible (Fig. 5, *b*) upon the addition of even small amounts of H_2O (~2%), $E_{(-)}^{2c}$ shifts to the region of

less negative values, and the limiting current of the second peak decreases appreciably compared to a similar value for the first peak with an increase in the water content. In the range $0 < V_{MeCN} < 0.5$, the second peak disappears (see Fig. 5, *c*). The result is unexpected: for the first time for compounds of the nitrone series we succeeded to observe the reversible one electron process in the first step of their electrochemical reduction in aqueous solutions and binary mixtures of the aprotic solvent—water type.

3.3 Radical anions and radical cations of 3,3´-bi(2-R-5,5-dimethy-1-4-oxopyrrolinylidene) 1,1´-dioxides

ESR spectra of the corresponding RA are detected under ECR at potentials of the first cathodic peaks ($E_{(-)}^{1c}$) [11] (Fig. 6). Corresponding isotropic hyperfine coupling constants (HFCC) are presented in Table 3. The character of the hyperfine structure of the ESR spectra of all RA generated in MeCN is the same as that for RA in DMF (Table 3, see ref. [10] also). Only a slight increase in the HFCC with ^{14}N nuclei is observed compared to the corresponding HFCC for RA in DMF. For RA **1** and **2**, all ^{19}F and ^{1}H nuclei of R substituents are spectrally equivalent and give septet hyperfine splitting with the binominal ratio of intensities of the components. At T = 298 K, no dynamic effects are observed, which are related to hindered rotation of the substituents in position 2 or torsional oscillations of the pyrrolinone moieties about the C=C bond when the solvent is replaced.

ESR spectra of the corresponding RC are observed under ECO of DN **2—4** at potentials of the first anodic peaks $E_{(+)}^{1a}$ (see Fig. 6). The nitrogen atoms of all RC are spectrally equivalent. A rather resolved hyperfine structure from protons of the substituents in position 2 of the pyrrolinone cycles is observed only for RC of methyl derivative **2** at T = 253 K, and the ESR spectra of RC **1** were not detected because of its instability (see Fig. 2, *a*). The HFCC of RC **2—4** are presented in Table 3.

Compound	R	Hyperfine coupling constants, mT	
		RA	RC
1	CF_3	0.462(^{14}N), 0.217(^{19}F) **0.444**(^{14}N)[c], **0.228**(^{19}F)	-
2	CH_3	0.414(^{14}N), 0.173(^{1}H) **0.408**(^{14}N), **0.174**(^{1}H)	0.141(^{14}N), 0.083(^{1}H)[b]
3	Ph	0.425(^{14}N) **0.433**(^{14}N)	0.150 (^{14}N)
4	t-Bu	0.435(^{14}N) **0.424**(^{14}N)	0.188(^{14}N)

a The radical anions were generated in MeCN at the corresponding potentials of the first reduction peak $E_{(-)}^{1c}$, and the radical cations were generated at the potential $E(+)^{1a}$; the concentration of the depolarizer and Et_4NClO_4 was $1.5 \cdot 10^{-3}$ and 0.1 mol/dm^3, respectively.
b The hyperfine structure 5N×7H becomes resolved at T < 253 K.
c HFCC in DMF.

Table 3. Comparative characteristics of the ESR spectra[a] of RA and RC **1—4** generated in MeCN and DMF (for RA) at 298 K.

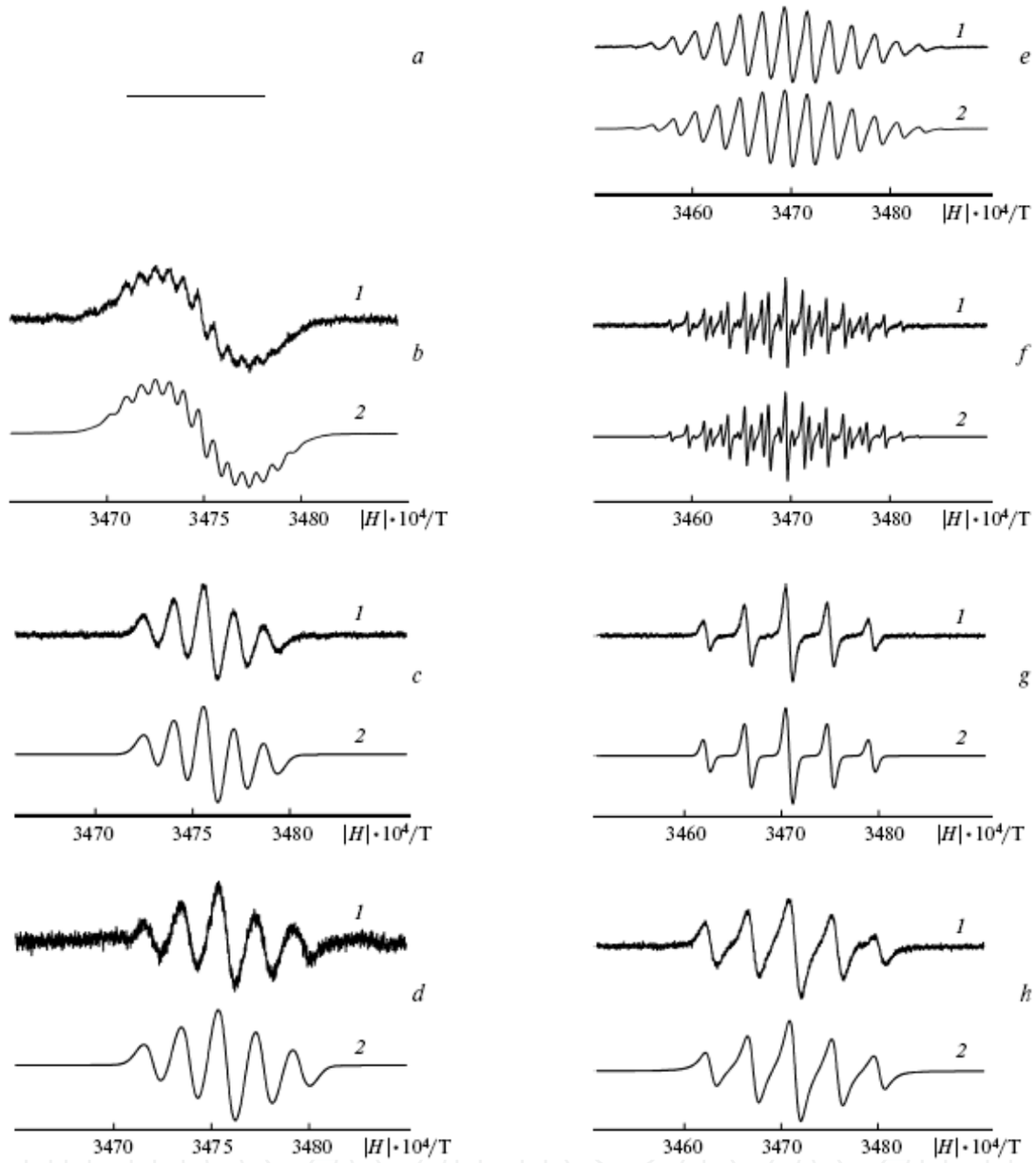

Fig. 6. ESR spectra of (*1*) RC (*a*—*d*) and RA (*e*—*h*) of dinitrones **1** (*a*, *e*), **2** (*b*, *f*), **3** (*c*, *g*), and **4** (*d*, *h*) generated by electrochemical oxidation and electrochemical reduction in MeCN (298 K) at the corresponding first peaks potentials and their numerical simulations (*2*).

On going from RA to the corresponding RC **2**—**4**, experimental values of nitrogen hyperfine splitting constant decreases, on the average, by 2.69 times (see Table 3), and the HFCC with the ^{1}H nuclei of the methyl groups (pair of RA **2**, RC **2**) decrease by 2.08 times. No HFCC with protons of the *tert*-butyl and phenyl groups are observed for both RA and RC **3** and **4**.

The ESR spectra of RA **1**—**4** were measured in MeCN—H_2O mixtures of various composition, which was characterized by the molar fraction of water (χ). Examples of the ESR spectra of RA **1**, **2**, **4** and their numerical simulations are given in Fig. 7. The maximum

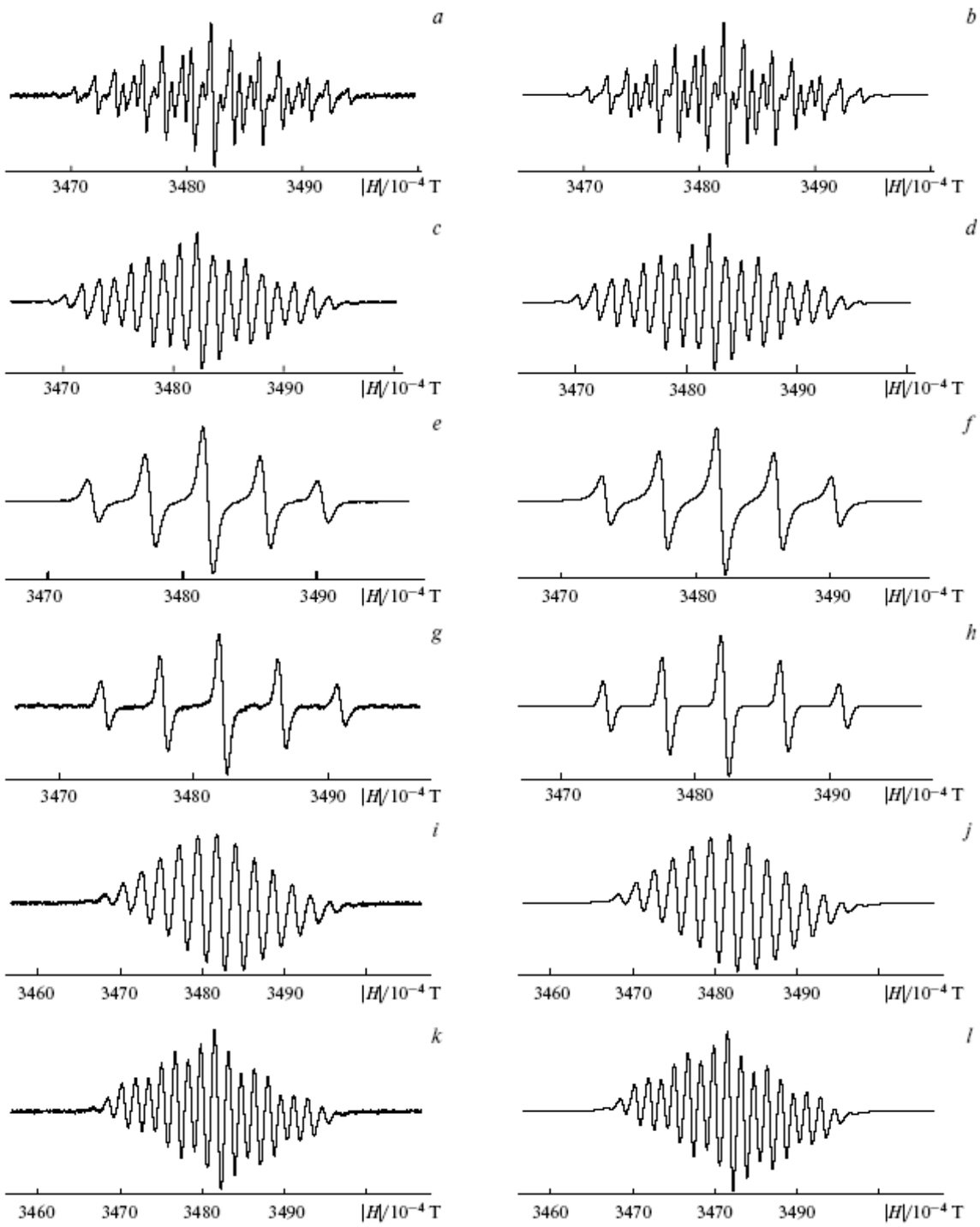

Fig. 7. The ESR spectra of RA **2** (*a* – *d*), **3** (*e* – *h*), and **1** (*i* – *l*) in MeCN and in MeCN – H_2O solvent mixture with maximum available content of H_2O: *a, c, e, g, i, k* are the experimental spectra, *b, d, f, h, j, l* are the numerical simulation of spectra; χ (molar fraction of H_2O) = 0 (*a, b, e, f, i, j*), 0.9 (*c*, *d*), 0.92 (*g*, *h*), and 0.5 (*k*, *l*).

value of χ in the mixture, at which the ESR spectra can be recorded, is not the same for nitrones **1**—**4** and is related to their different solubility [13]. For DN **2** possessing the highest solubility, the ESR spectra of the corresponding RA can be recorded within entire range of the MeCN—H_2O composition. The *g*-factors of RA **1**—**4** are close (2.0032±0.0004) and virtually do not depend on the mixture composition. The HFCC of RA **1**—**4** in MeCN and at the highest possible values of χ are given in Table 4. The well resolved hyperfine structure (HFS) on the ^{1}H and ^{19}F nuclei of substituents R are observed for RA **2** and **1** within entire available range of the mixture compositions. For RA **3** and **4**, only HFS on the ^{14}N nuclei are observed due to the remoteness of the substituents R protons, which is in agreement with the published data [11].

The dependencies of the HFCC for RA **1**—**4** on χ are shown in Fig. 8. For RA **1** and **2**, the nitrogen HFCC (a_N) increase with the increase of χ, the proton (a_H) and fluorine (a_F) HFCC constants change in opposite direction to the dependence of $a_N(\chi)$ (see Fig. 8, *a*—*c*). The solvation curves for all three types of the HFCC of RA **1** and **2** are well described by the empirical exponential functions of the form as follows:

$$a_{ki}(\chi) = a_{ki}(1) + S_{ki} \exp(-K_{ki}\chi), \quad (4)$$

where k = ^{14}N, ^{19}F, ^{1}H, i is the RA's number. Parameters S_{ki} and K_{ki} for RA **1** and 2 are given in Table 5. The dependencies $a_N(\chi)$ for RA **3** and **4** sharply differ (see Fig. 8, *d*): for RA **3** (R = Ph) $a_N(\chi)$ has the S-like form qualitatively similar to the solvation dependencies of the nitrogen HFCC for RA of some *ortho*-substituted nitrobenzenes [14], whereas the solvent function $a_N(\chi)$ for RA **4** (R = Bu^t) has the minimum at χ = 0.3.

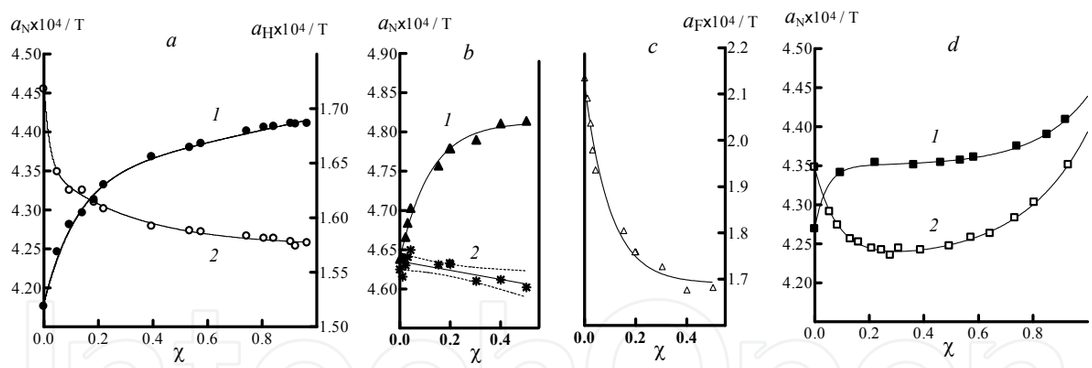

Fig. 8. Hyperfine coupling constants *versus* molar fraction of water (χ): (*a*) RA **2** (*1* — a_N, *2* — a_H); (*b*), (*c*) RA **1**, (*b*): a_N (*1*), the difference of experimental values and resolvation contribution for RA **1** ($a_N(\chi) - \Delta a_N^{solv}(\chi)$ (*2*), (*c*): a_F; (*d*): a_N for RA **3** (*1*), **4** (*2*).

R / *k*	CF_3 (**1**)		CH_3 (**2**)		Ph (**3**)		Bu^t (**4**)	
	χ=0	χ=0.50	χ=0	χ=0.97	χ=0	χ=0.93	χ=0	χ=0.92
^{14}N	4.638	4.814	4.176	4.406	4.269	4.409	4.348	4.351
^{1}H	—	—	1.718	1.581	—		—	
^{19}F	2.137	1.682	—	—	—		—	

Table 4. The HFCC (a_k×10^4 T) of RA of 3,3′-bi(2-R-5,5-dimethyl-4-oxopyrrolinylidene) 1,1′-dioxides **1**—**4** in MeCN—H_2O solvent mixtures.

k / R	^{14}N			^{19}F			^{1}H		
	a_{ki}(1)	S_{ki}	K_{ki}	a_{ki}(1)	S_{ki}	K_{ki}	a_{ki}(1)	S_{ki}	K_{ki}
CF_3 (**1**)	4.813	–0.176	8.310	1.687	0.438	10.874	—	—	—
CH_3 (**2**)	4.408	–0.219	4.716	—	—	—	1.582	0.129	8.803

Table 5. Parameters of empirical solvent dependencies (4) for RA **1** and **2** ([a_{ki}(1)], [S_{ki}] = $\times 10^4$ T=G).

3.4 Spacial, electronic structures of 3,3´-bi(2-R-5,5-dimethy-1-4-oxopyrrolinylidene) 1,1´-dioxides molecular ions and interpretation of hyperfine coupling constants solvent dependences for radical anions.

Semiempirical UHF and RHF calculations with PM3 Hamiltonian of the geometric parameters of the neutral species and molecular ions of **1—4** in the ground state show that all structures have the C_2 symmetry. In the molecular ions, both pyrrolinone cycles are planar in fact, and the angle between the cycles (θ_0) in optimized conformations increases with an increase in the effective volume of substituent R (Table 6.), whereas the θ_0 values are higher than those for the neutral species and increase with an increase in the ion charge.

According to the UHF/PM3 calculations [11] for both types of paramagnetic ions **2—4**, the ^{14}N nuclei in the pyrrolinone cycles should be spectrally equivalent, which is confirmed by experiment. The corresponding spin site occupancies of the 2s-AOs of the nitrogen atoms are the following: ($S_{2s\text{-}AO}$(RA **2**), $S_{2s\text{-}AO}$(RC **2**)) = (0.02166,–0.00181);

Com-pound	R	$\theta_{0(n)}$		$\theta_{0(RC)}$		$\theta_{0(DC)}$		$\theta_{0(RA)}$		$\theta_{0(DA)}$	
		UHF	RHF	UHF	RHF	UHF	RHF	UHF	RHF	UHF	RHF
1	CF_3	44.2	30.8	47.6	47.6	—	—	45.9	47.7	89.8	89.8
2	CH_3	38.2	30.1	36.6	36.7	39.3	42.7	37.0	37.4	41.4	43.9
3	Ph	63.6	37.2	47.8	48.7	58.2	73.9	67.7	56.0	86.6	80.6
4	Bu^t	—[a]	55.1	88.0	72.1	86.9	86.9	62.7	72.7	—[a]	—[a]

Table 6. Dihedral angles (θ_0/deg) between the pyrrolinone cycles in neutral DN **1—4** and their molecular ions according to the data of PM3 calculations in the UHF and RHF approximations.

($S_{2s\text{-}AO}$(RA **3**), $S_{2s\text{-}AO}$(RC **3**)) = (0.02354,–0.00196); ($S_{2s\text{-}AO}$(RA **4**), and $S_{2s\text{-}AO}$(RC **4**)) = (0.02314,–0.00125). Therefore, the calculation predicts qualitatively the close constants in the series of RC **2—4** and RA **2—4** and a considerable decrease in the a_N constant on going from RA to RC due to the redistribution of spin density from nitrogen to oxygen atoms of nitrone groups.

This fact is confirmed by more sophisticated UB3LYP method with 6-31+G* basis set for the gaseous phase in the pair RA-RC of DN **2** as an example. Corresponding spin density distributions are shown in Fig. 9.

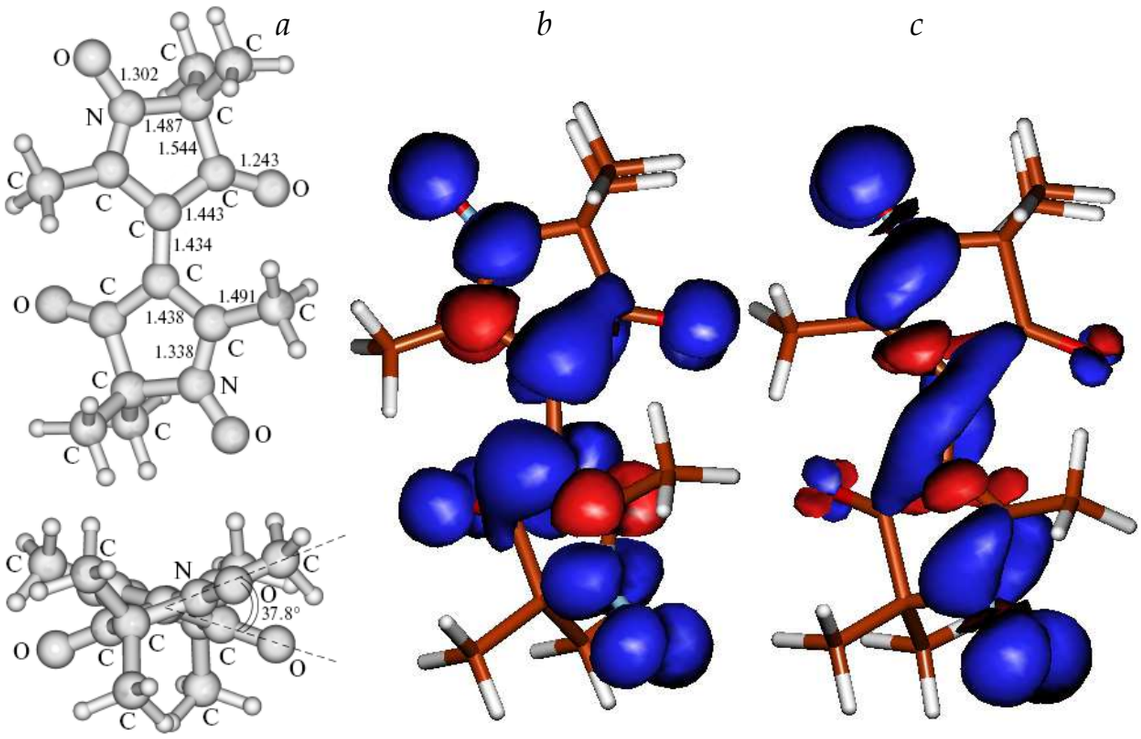

Fig. 9. The equilibrium conformation of RA **2** (*a*), distributions of the spin density in RA **2** (*b*) and RC **2** (*c*) according to the UB3LYP/6-31+G* data for the gaseous phase (blue color – positive sign of spin density, red – negative sign).

The angle θ_0 and HFCC values for RA **2** in the gaseous phase and with allowance for the medium using the PCM model are given in Table 7. According to the calculations, the HFCC with the protons of the methyl group in position 2 are negative, whereas with the ^{14}N nuclei, positive. Transition from the gaseous phase to the liquid causes insignificant increase of the angle θ_0 and nitrogen HFCC (Table 7) and decrease of the proton constant. On the increase of the dielectric permittivity of the medium from 36.64 (MeCN) to 78.39 (H_2O), the turning angle between the rings remains virtually unchanged.

The nitrogen HFCC calculated with allowance for the medium are close to the experimental values, whereas the proton HFCC are by 1.5 times larger than experimental. According to UB3LYP/6-31+G*/PCM calculations the change of the medium virtually has no effect on the values of both HFCC.

Let us suggest that starting from the results of calculation of RA **2** by the UB3LYP method, the shape of the experimental solvation dependence $a_N(\chi)$ for RA **2** is caused only by the change of the solvate cage upon increase of χ. In this case, the function

$$a_{N2}(\chi) - a_{N2}(0) = \Delta a_{N2} + S_{N2}\exp(-K_{N2}\cdot\chi) = \Delta\, a_N^{solv}(\chi) \quad (5)$$

Phase	ε^a	r_{solv} / Å^b	θ_0 / deg	$a_N^{UB3LYP} \times 10^4$, T	$< a_H^{UB3LYP} > \times 10^4$, T^c
Gaseous	1	-	37.81	3.848	–2.705
MeCN (PCM)	36.64	3.720	42.48	3.962	–2.549
H_2O (PCM)	78.39	1.385	39.84	3.964	–2.544

a Dielectric constants in the PCM calculations.
b Effective radius of the solvent.
c Average dynamic value: $< a_H^{UB3LYP} > = (1/3)(\sum_{j=1}^{3} \rho_H(r_j))A_H$, where $\rho_H(r_j)$ are spin densities at the protons of the methyl groups at position 2, A_H = 159.22 mT is the atomic constant for the proton.

Table 7. The HFCC and angles θ_0 in the equilibrium conformations of RA **2** from the UB3LYP/6-31+G* calculation data in the gaseous phase and with simulation of the liquid phase in the framework of the PCM model.

where $\Delta a_{N2} = a_{N2}(1) - a_{N2}(0)$, can be approximately considered as general «resolvation contribution» into the dependence of $a_N(\chi)$ for all RA **1—4,** which is related only to the resolvation without conformational change. In such a case, for the RA of trifluoromethyl derivative **1** the following equality should take place:

$$a_{N1}(\chi) - \Delta a_N^{solv}(\chi) \approx \text{const}, \quad (6)$$

which, in fact, is observed with the accuracy to 0.005 mT in the range $0 < \chi < 0.5$ (see Fig. 8, *b*). This means that for RA **1**, the angle θ is virtually constant, at least in the range of χ studied, whereas the absence of the structural contribution $a_N(\theta,\chi)$ into the solvent dependences of the nitrogen constants for RA **1** and **2** in the range of χ studied explains their similar shape (see Fig. 8, *a*, *b*).

We will evaluate the contributions $a_N(\theta,\chi)$ for RA **3** and **4** related to the change of θ starting from the calculations of the angular functions of the nitrogen constants by the DFT/PBE method [15] in the basis 3z* and experimental dependences of the constants with allowance for the resolvation contribution $\Delta a_N^{solv}(\chi)$. The results of calculation of angles θ_0 and corresponding HFCC in the equilibrium conformations of RA **1—4** are given in Table 8.

For RA **2**, the DFT/PBE calculations on average twice underestimate the nitrogen constant values as compared to the UB3LYP calculations (*cf.* with the data in Table 7), but in the series of RA **1—4** they correctly indicate the tendency of the change of a_N measured in MeCN despite small values of their absolute changes. The relations of experimental and calculated constants $R_i = a_{Ni} / a_{Ni}^{PBE}$ are given in Table 8.

Since all the RA possess different values of θ_0, it is convenient to introduce the value $\phi = \theta - \theta_0$ as an argument of the angular functions. According to the calculations in the range $-30° < \phi < 30°$, the angular functions of the nitrogen constants are linear:

$$a_{Ni}^{PBE}(\phi) = A_i + B_i\phi \quad (7)$$

* 3z basic set {3, 1, 1/1} for H and {6, 1, 1, 1, 1, 1/1} for C, N, O, F [15].

RA	θ_0/deg	a_{Ni}^{PBE} ×10⁴/ T	$< a_{Fi}^{PBE} >^a$ ×10⁴ / T	$< a_{Hi}^{PBE} >^a$, ×10⁴/ T	R_i	A_i×10⁴ / T	B_i×10⁴ / T / deg	r[b]
1	43	1.7 95	–1.715	—	2.512	—	—	—
2	38	1.584	—	–1.233	2.637	—	—	—
3	40.8	1.764	—	—	2.420	1.764	–0.006638	0.998
4	52	1.731	—	—	2.512	1.731	–0.005723	0.997

a The HFCC with ^{19}F and ^{1}H nuclei of CF_3 and Me groups are the dynamic average values.
b Correlation coefficients of the linear regressions (7).

Table 8. The HFCC, relationship of experimental and calculated nitrogen constant values (R_i), angles θ_0 in the equilibrium conformations of RA **1—4**, as well as parameters of the angular dependencies (7) from the DFT/PBE calculation data.

Parameters A_i, B_i of regressions (7) and the corresponding correlation coefficients are given in Table 8. Multipliers B_i are negative, *i.e.* an increase of θ leads to the decrease of the nitrogen HFCC and to the redistribution of the spin density involving the O atoms of the nitrone groups.

The structurally dependent solvation contributions for RA **3** and RA **4** are determined as follows:

$$a_{Ni}(\theta,\chi) = a_{Ni}(\chi) - \Delta a_N^{solv}(\chi) = R_i[A_i + B_i\phi_i(\chi)] \quad (8)$$

Direct calculations lead to the qualitatively similar functions $\phi_i(\chi)$ differing in the angular amplitude and behavior in the starting sections. They are shown in Fig 10. The maximum deviations of the angles for RA **3** and **4** are ~8 and ~22°, respectively. The maxima of $\phi_i(\chi)$ for both RA are very close and correspond to $\chi \approx 0.5$. An increase in the content of water in the mixture MeCN—H_2O leads to the different behavior of the angular functions $\phi_i(\chi)$ in the starting regions ($0 < \chi < 0.2$, see Fig. 11) and, therefore, to the domination of different contributions for RA **3** and **4**. In the solvent dependence $a_{N2}(\chi)$ for RA **3** in this range of molar fractions, the resolvation contribution is predominant, that leads to a sharp increase of a_N (see Fig.8, *d*), whereas at $\chi > 0.5$, the structural contribution dominates, that finally leads to an S-figurative general solvent function $a_{N2}(\chi)$. For RA **4** containing substituent of larger effective size (But) and possessing maximum noncoplanarity ($\theta_0 = 52°$), the situation is reverse, and the function $a_{N3}(\chi)$ has the minimum (see Fig. 8, *d*). RA **1** and **2** contain substituents of small effective size (CF_3 and Me groups) and, according to the given estimates, do not undergo noticeable distortions, whereas the shape of functions $a_{N1,2}(\chi)$ is due to the redistribution of the π-spin density from the atoms C(2), C(2′) to the atoms N and O (see Fig. 10) of the nitrone groups upon increase in water content.

4. Concluding remarks

Thus, generalizing the results of our studies (see [10, 11, 13] also) one can assert, that we described the electrochemical behavior of the new class of heterocyclic compounds of the nitrone series with a very high electron withdrawing ability capable of forming long-lived molecular ions in aprotic media. The electrochemical behavior of the But substituted dinitrone is unique: the EE processes within one cycle of potential sweep in cyclic voltammogram

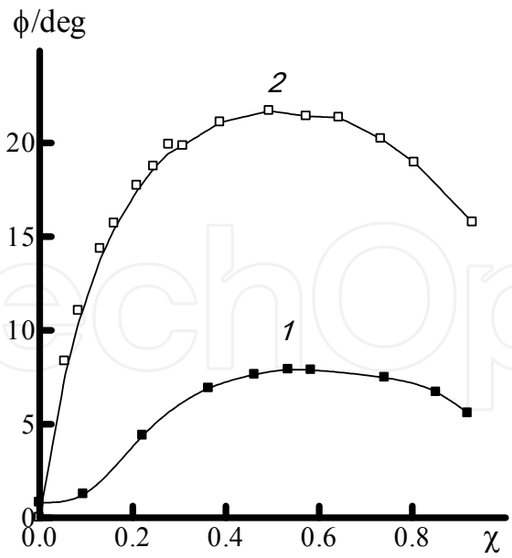

Fig. 10. The turning angle of pyrrolinone cycles for RA **3** (*1*) and **4** (*2*) *versus* molar fraction of water in the binary MeCN—H_2O mixtures.

were observed in both regions of negative and positive potentials with the formation of dianion, radical anion, radical cation, and dication, which are long-lived at T = 298 K.

Radical anions of dinitrones, which are long-lived in aprotic solvents and their mixtures with water have been described for the first time. The differences in solvent dependencies of hyperfine coupling constants with ^{14}N nuclei were explained based on the assumption on competition of resolvation and structural effects upon increase in H_2O content in the binary mixture MeCN-H_2O.

The corresponding values of the first peaks potentials of DN's **1-4** ECR in water are rather low and close to the redox potentials of the ferrocene derivatives, which are widely used in the recent time as redox-active labels in electrochemical detection of nucleic acid hybridization [16, 17] particularly, for the development of DNA microarrays with electrochemical detection of hybridization [18]. We believe that the dinitrone derivatives, which possess low potentials of electrochemical reduction and contain appropriate active groups (substituents) capable of binding with DNA, can be rather efficient redox-active labels for the electrochemical detection of DNA hybridization when the double DNA chain does not undergo irreversible destruction. Our recent study was devoted to the development of synthetic method of introduction such substituents in the described dinitrones for this aim [19].

4. Acknowledgment

We thank the Russian Foundation for Basic Research for financial support of this work (Project No. 10-03-00844-a).

5. References

[1] I.A. Grigor'ev, G.I. Shchukin, V.V. Khramtsov, L.M. Vainer, and V.F. Starichenko // *Russ. Chem. Bull., Int. Ed.*, 1985,. 34, 2169.

[2] Eberson L. // *J. Chem. Soc. Perkin Trans. 2*., 1992, 1807-1813.
[3] K. Nishikida, T. Kubota, H. Miyazaki, and S. Sakata, // *J. Magn. Reson.*, 1972, 7, 260.
[4] H. Miyazaki, T. Kubota, and Y. Matsuhisa, *Bull. Chem. Soc. Jpn.*, 1981, 54, 3850.
[5] H. Miyazaki, T. Kubota, and M. Yamakawa, *Bull. Chem.Soc. Jpn.*, 1972, 45, 780.
[6] I.M. Sosonkin, V. N. Belevskii, G. N. Strogov, A. N. Domarev, and S. P. Yarkov, *Zh. Org. Khim.*, 1982, 18, 1504 [*J. Org. Chem. USSR*, 1982, 18, 1313 (Engl. Transl.)].
[7] T. H. Walter, E. E. Bankroft, G. L. McIntire, E. R. Davis,L. M. Gierasch, H. N. Blount, H. J. Stronks, and E. V. Janzen, *Can. J. Chem.*, 1982, 60, 1621.
[8] K. Ashok, P. M. Scaria, P. V. Kamat, and M. George, *Can. J. Chem.*, 1987, 65, 2039.
[9] G. L. McIntire, H. N. Blount, H. J. Stronks, R. V. Shetty, and E. V. Janzen, *J. Phys. Chem.*, 1980, 84, 916.
[10] L. A. Shundrin, V. A. Reznikov, I. G. Irtegova, and V. F. Starichenko *// Russ. Chem. Bull., Int. Ed.*, 2003,. 52, 939.
[11] L. A. Shundrin, I. G. Irtegova, A. D. Rogachev, and V. A. Reznikov *// Russ. Chem. Bull., Int. Ed.*, 2005, 54, 1178.
[12] A.S. Morkovnik and O. Yu. Okhlobystin // *Chem. Heterocycl. Compd.*, 1980, 16, No. 8, 777.
[13] L. A. Shundrin, N. V. Vasil'eva, I. G. Irtegova, V. A. Reznikov //*Russ. Chem. Bull., Int. Ed.,* 2007, 56, 1273.
[14] L. A. Shundrin, V. F. Starichenko, L. N. Shchegoleva, V. D. Shteingarts // *J. Sruct. Chem.*, 2003, 44(4), 592.
[15] D. N. Laikov, *Chem. Phys. Lett.*, 1997, 281, 151.
[16] T. S. Zatsepin, S. Yu. Andreev, T. Gianik, and T. S. Oretskaya, // *Russ. Chem. Rev.*, 2003, 72, 537.
[17] A.Anne, A. Bouchardon, and J. Moiroux, *J. Am. Chem. Soc.*, 2003, 125, 1112.
[18] S. Abramowitz, *J. Biomed. Dev.*, 1999, 1, 107.
[19] I.A. Khalfina, N. V. Vasil'eva, I. G. Irtegova, L. A. Shundrin, and V. A. Reznikov // *Russ. J. Org. Chem., 2010,* 46*, 399.*

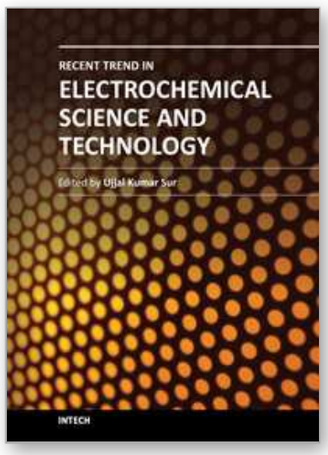

Recent Trend in Electrochemical Science and Technology

Edited by Dr. Ujjal Kumar Sur

ISBN 978-953-307-830-4
Hard cover, 306 pages
Publisher InTech
Published online 27, January, 2012
Published in print edition January, 2012

This book titled "Recent Trend in Electrochemical Science and Technology" contains a selection of chapters focused on advanced methods used in the research area of electrochemical science and technologies; descriptions of electrochemical systems; processing of novel materials and mechanisms relevant for their operation. This book provides an overview on some of the recent development in electrochemical science and technology. Particular emphasis is given both to the theoretical and the experimental aspect of modern electrochemistry. Since it was impossible to cover the rich diversity of electrochemical techniques and applications in a single issue, the focus is on the recent trends and achievements related to electrochemical science and technology.

InTech Europe
University Campus STeP Ri
Slavka Krautzeka 83/A
51000 Rijeka, Croatia
Phone: +385 (51) 770 447
Fax: +385 (51) 686 166
www.intechopen.com

InTech China
Unit 405, Office Block, Hotel Equatorial Shanghai
No.65, Yan An Road (West), Shanghai, 200040, China
中国上海市延安西路65号上海国际贵都大饭店办公楼405单元
Phone: +86-21-62489820
Fax: +86-21-62489821

IntechOpen